

Numerical Study of the Ghost-Gluon Vertex in Landau gauge

A. Cucchieri, T. Mendes and A. Mihara

Instituto de Física de São Carlos – Universidade de São Paulo

C.P. 369, 13560-970 São Carlos, SP – Brazil

(Dated: August 24, 2004)

Abstract

We present a numerical study of the ghost-gluon vertex and of the corresponding renormalization function $\tilde{Z}_1(p^2)$ in minimal Landau gauge for $SU(2)$ lattice gauge theory. Data were obtained for three different lattice volumes ($V = 4^4, 8^4, 16^4$) and for three lattice couplings $\beta = 2.2, 2.3, 2.4$. Gribov-copy effects have been analyzed using the so-called smeared gauge fixing. We also consider two different sets of momenta (orbits) in order to check for possible effects due to the breaking of rotational symmetry. The vertex has been evaluated at the asymmetric point $(0; p, -p)$ in momentum-subtraction scheme. We find that $\tilde{Z}_1(p^2)$ is approximately constant and equal to 1, at least for momenta $p \gtrsim 1$ GeV, confirming the well-known perturbative result. Finally, we use our data to evaluate the running coupling constant $\alpha_s(p^2)$.

I. INTRODUCTION

In the framework of quantum field theory, Faddeev-Popov ghosts are introduced in order to quantize non-Abelian gauge theories. Although the ghosts are a mathematical artifact and are absent from the physical spectrum, one can use the ghost-gluon vertex and the ghost propagator to calculate physical observables, such as the QCD running coupling $\alpha_s(p^2)$, using the relation [1]

$$\alpha_s(p^2) = \alpha_0 \frac{Z_3(p^2) \tilde{Z}_3^2(p^2)}{\tilde{Z}_1^2(p^2)}. \quad (1)$$

Here $\alpha_0 = g_0^2/4\pi$ is the bare coupling constant and $Z_3(p^2)$, $\tilde{Z}_3(p^2)$ and $\tilde{Z}_1(p^2)$ are, respectively, the gluon, ghost and ghost-gluon vertex renormalization functions.

The above formula gets simplified if one considers the Landau gauge. Indeed, in this case the vertex renormalization function $\tilde{Z}_1(p^2)$ is finite and constant, i.e. independent of the renormalization scale p , at least to all orders of perturbation theory (see [2] and the nonrenormalization theorems in [3, Chapter 6]). Of course, it is important to verify in a non-perturbative way that this result really holds. If it does, one can consider in the Landau gauge a definition of the running coupling constant that requires only the calculation of the gluon and ghost propagators [4, 5]. Let us recall that in Landau gauge these propagators can be expressed (in momentum space) as

$$D_{\mu\nu}^{bc}(q, -q) = \delta^{bc} \left(\delta_{\mu\nu} - \frac{q_\mu q_\nu}{q^2} \right) D(q^2) = \delta^{bc} \left(\delta_{\mu\nu} - \frac{q_\mu q_\nu}{q^2} \right) \frac{F(q^2)}{q^2} \quad (2)$$

$$G^{bc}(q, -q) = -\delta^{bc} G(q^2) = -\delta^{bc} \frac{J(q^2)}{q^2}, \quad (3)$$

where $F(q^2)$ and $J(q^2)$ are, respectively, the gluon and ghost form factor and the color indices b and c take values $1, 2, \dots, N_c^2 - 1$ in the $SU(N_c)$ case. Then, in the momentum-subtraction scheme one has that the gluon and ghost renormalization functions are given by

$$F_R(q^2, p^2) = Z_3^{-1}(p^2) F(q^2) \quad (4)$$

$$J_R(q^2, p^2) = \tilde{Z}_3^{-1}(p^2) J(q^2) \quad (5)$$

with the renormalization conditions

$$F_R(p^2, p^2) = J_R(p^2, p^2) = 1. \quad (6)$$

Thus, after setting $\tilde{Z}_1(p^2) = 1$, the running coupling (1) can be written as [4, 5]

$$\alpha_s(p^2) = \alpha_0 F(p^2) J^2(p^2), \quad (7)$$

i.e. one only needs to evaluate the gluon and ghost form factors defined above. In recent years, the infrared behavior of these form factors has been extensively studied (in Landau gauge) using different analytical approaches [4, 5, 6, 7, 8, 9, 10, 11, 12, 13, 14, 15, 16, 17, 18, 19, 20, 21, 22, 23, 24]. Also, numerical studies of these form factors and of the running coupling defined in eq. (7) have been reported in [25, 26, 27, 28] for the $SU(2)$ group and in [29, 30, 31, 32, 33, 34, 35, 36] for the $SU(3)$ case.

An indirect evaluation of the ghost-gluon vertex renormalization function has been recently presented in [28], confirming that $\tilde{Z}_1(p^2)$ is finite in the continuum limit. On the other hand, a direct nonperturbative verification of this result from a numerical evaluation of the ghost-gluon vertex is still missing. Let us stress that a direct evaluation of $\tilde{Z}_1(p^2)$ would allow a study of the running coupling constant [37] using eq. (1) instead of eq. (7). Such a study may improve the precision of the determination of $\alpha_s(p^2)$, since in that case one does not need, in principle, to use the so-called *matching rescaling* technique [28] when considering data obtained at different β values.

In this paper we study numerically the ghost-gluon vertex and the corresponding renormalization function $\tilde{Z}_1(p^2)$ for the $SU(2)$ case in the minimal Landau gauge. The definition of this renormalization function (in the continuum) is presented in Section II. Numerical simulations are explained in Section III. In particular, in Section III A we define the vertex renormalization function on the lattice and compare our direct determination of $\tilde{Z}_1(p^2)$ to the indirect evaluation presented in [28]. Results for the ghost-gluon vertex renormalization function, the gluon and ghost propagators and the running coupling constant $\alpha_s(p^2)$ are reported in Section IV. Finally, in Section V we draw our conclusions. Preliminary results have been reported in [38].

II. THE GHOST-GLUON VERTEX

Following the notation in Ref. [39] (see also Fig. 1) the 3-point function for A_μ^a (gluon), η^b (ghost) and $\bar{\eta}^c$ (anti-ghost) fields — corresponding to the ghost-gluon vertex — is given

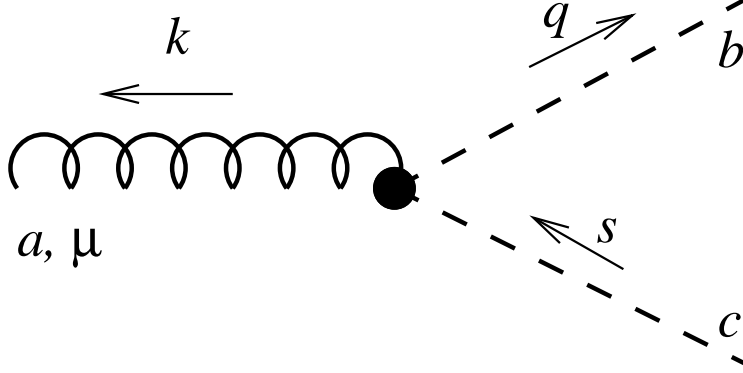


Figure 1: Notation (momenta and indices) for the ghost-gluon vertex.

by

$$V_\mu^{abc}(x, y, z) = \langle A_\mu^a(x) \eta^b(y) \bar{\eta}^c(z) \rangle . \quad (8)$$

Going to momentum space and using translational invariance for the 3-point function, one gets

$$V_\mu^{abc}(k; q, s) = \int d^4x d^4y d^4z e^{-i(kx+qy-sz)} V_\mu^{abc}(x, y, z) \quad (9)$$

$$= \int d^4z e^{-i(k+q-s)z} \int d^4x d^4y e^{-i(kx+qy)} \langle A_\mu^a(x) \eta^b(y) \bar{\eta}^c(0) \rangle \quad (10)$$

$$= (2\pi)^4 \delta^4(k+q-s) G_\mu^{abc}(k, q) , \quad (11)$$

where $\delta^4(k+q-s)$ implies conservation of momentum. Then, the ghost-gluon vertex function is obtained by “amputating” the corresponding 3-point function (see Fig. 2)

$$\Gamma_\mu^{abc}(k, q) = \frac{G_\mu^{abc}(k, q)}{D(k^2) G(q^2) G(s^2)} , \quad (12)$$

where $s = k + q$ and the functions $D(k^2)$ and $G(q^2)$ have been defined in eqs. (2) and (3), respectively. At tree level (in the continuum) one obtains [1]

$$\Gamma_\mu^{abc}(k, q) = i g_0 f^{abc} q_\mu , \quad (13)$$

where g_0 is the bare coupling and f^{abc} are the structure functions of the $SU(N_c)$ Lie algebra. This implies the well-known result that the ghost-gluon vertex is proportional to the momentum q of the outgoing ghost. More generally, we can write the relation [39]

$$\Gamma_\mu^{abc}(k, q) = g_0 f^{abc} \Gamma_\mu(k, q) , \quad (14)$$

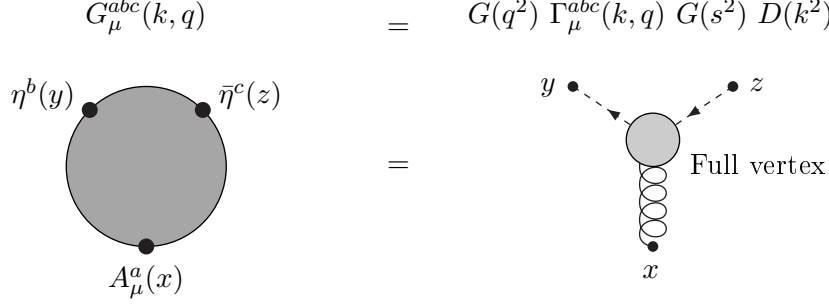


Figure 2: The 3-point function $G_\mu^{abc}(k, q)$ and its relation with the full ghost-gluon vertex $\Gamma_\mu^{abc}(k, q)$.

where $\Gamma_\mu(k, q)$ is the so-called reduced vertex function. Then, multiplying the previous equation by $f^{dbc} \delta^{ad}$, summing over a, b, c, d and using the relation $\sum_{b,c} f^{dbc} f^{abc} = N_c \delta^{da}$ we get

$$\Gamma_\mu(k, q) = \frac{1}{g_0 N_c (N_c^2 - 1)} \sum_{a,b,c} f^{abc} \Gamma_\mu^{abc}(k, q) . \quad (15)$$

Since at tree level one has $\Gamma_\mu(k, q) = i q_\mu$ we can also write

$$\Gamma_\mu(k, q) = i q_\mu \Gamma(k^2, q^2) \quad (16)$$

and it is the scalar function $\Gamma(k^2, q^2)$ that gets renormalized, when considering a given renormalization scheme. Clearly, from the above relations we obtain

$$\Gamma(k^2, q^2) = \frac{-i}{q^2} \sum_\mu q_\mu \Gamma_\mu(k, q) = \frac{-i}{g_0 N_c (N_c^2 - 1)} \frac{1}{q^2} \sum_\mu q_\mu \sum_{a,b,c} f^{abc} \Gamma_\mu^{abc}(k, q) . \quad (17)$$

In our simulations we considered the asymmetric point with zero momentum for the gluon ($k = 0$), implying $s = q$. Formula (17) then becomes

$$\Xi(q^2) = \Gamma(0, q^2) = \frac{-i}{g_0 N_c (N_c^2 - 1)} \frac{1}{q^2} \sum_\mu q_\mu \sum_{a,b,c} f^{abc} \Gamma_\mu^{abc}(0, q) . \quad (18)$$

Let us note that the factor $-i$ in the equations above disappears, since only the imaginary part of the vertex function $\Gamma_\mu^{abc}(0, q)$ contributes to the quantity $\Xi(q^2)$, i.e. we can write

$$\Xi(q^2) = \frac{1}{g_0 N_c (N_c^2 - 1)} \frac{1}{q^2} \sum_\mu q_\mu \sum_{a,b,c} f^{abc} \text{Im} \Gamma_\mu^{abc}(0, q) . \quad (19)$$

Finally, in momentum-subtraction scheme one fixes the vertex renormalization function $\tilde{Z}_1(p^2)$ by requiring (see also Fig. 3)

$$\Xi_R(q^2, p^2) = \tilde{Z}_1(p^2) \Xi(q^2) \quad (20)$$

$$\Xi_R(p^2, p^2) = 1 , \quad (21)$$

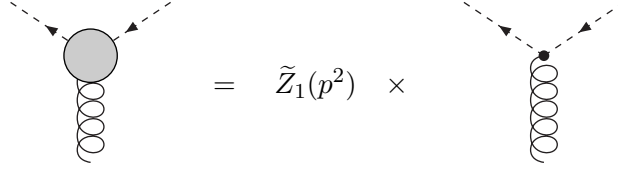


Figure 3: Relation between the full (left) and the bare (right) vertices.

namely the renormalized reduced vertex function $\Gamma_\mu(0, q)$ is equal to the tree-level value $i q_\mu$ at the renormalization scale. Then, the vertex renormalization function is given by

$$\tilde{Z}_1^{-1}(p^2) = \Xi(p^2) . \quad (22)$$

We also obtain that the running coupling can be written as

$$g_s(p^2) = g_0 \tilde{Z}_1^{-1}(p^2) Z_3^{1/2}(p^2) \tilde{Z}_3(p^2) \quad (23)$$

$$= g_0 \Xi(p^2) F^{1/2}(p^2) J(p^2) \quad (24)$$

$$= \frac{1}{N_c(N_c^2 - 1)} \frac{F^{1/2}(p^2) J(p^2)}{p^2 D(0) G^2(p^2)} \sum_\mu p_\mu \sum_{a,b,c} f^{abc} \text{Im } G_\mu^{abc}(0, p) \quad (25)$$

$$= \frac{1}{N_c(N_c^2 - 1)} \frac{F^{1/2}(p^2)}{D(0) G(p^2)} \sum_\mu p_\mu \sum_{a,b,c} f^{abc} \text{Im } G_\mu^{abc}(0, p) , \quad (26)$$

where we used eq. (3).

III. NUMERICAL SIMULATIONS

For the simulations (see [40] for details) we consider the standard Wilson action, thermalized using heat-bath [41] accelerated by *hybrid overrelaxation* [42, 43, 44]. Since we are considering the $SU(2)$ gauge group we parametrize the link variables $U_\mu(x)$ as

$$U_\mu(x) = u_\mu^0(x) \mathbb{1} + i \vec{u}_\mu(x) \vec{\sigma} , \quad (27)$$

where $\mathbb{1}$ is the 2×2 identity matrix, σ^b are the Pauli matrices and the relation

$$[u_\mu^0(x)]^2 + [\vec{u}_\mu(x)]^2 = 1 \quad (28)$$

is satisfied. We also consider the standard definition of the lattice gluon field, i.e.

$$A_\mu(x) = A_\mu^b(x) \sigma^b = \frac{U_\mu(x) - U_\mu^\dagger(x)}{2i} , \quad (29)$$

Lattice Volume $V = N^4$	4^4	8^4	16^4
No. of Configurations	1000	400	250

Table I: Lattice volumes and total number of configurations considered.

implying that the lattice gluon field component $A_\mu^b(x)$ is equal to $u_\mu^b(x)$. The connection between the lattice link variables $U_\mu(x)$ and the continuum gauge field $A_\mu(x)$ is given by

$$U_\mu(x) = \exp \left[i a g_0 A_\mu^b(x) t^b \right], \quad (30)$$

where $t^b = \sigma^b/2$ are the generators of the SU(2) algebra, a is the lattice spacing and g_0 is the bare coupling constant. Then, the lattice quantity $2 A_\mu^b(x)/(a g_0)$ approaches the continuum-gluon-field component $A_\mu^b(x)$ in the naive continuum limit $a \rightarrow 0$. Let us also recall that a generic lattice momentum \hat{q} has components (in lattice units)

$$\hat{q}_\mu = 2 \sin \left(\frac{\pi \tilde{q}_\mu a}{L_\mu} \right). \quad (31)$$

Here $L_\mu = a N_\mu$ is the physical size of the lattice in the μ direction, the quantity \tilde{q}_μ takes values $\lfloor \frac{-N_\mu}{2} \rfloor + 1, \dots, \lfloor \frac{N_\mu}{2} \rfloor$ and N_μ is the number of lattice points in the μ direction. If we keep the physical size L_μ constant and indicate with q_μ the momentum components in the continuum, we find that the lattice components $\hat{q}_\mu = a q_\mu$ take values in the interval $(-\pi, \pi]$ when $a \rightarrow 0$.

In Table I we show the lattice volumes used in the simulations and the corresponding numbers of configurations. For each volume we have considered three values of the lattice coupling, namely $\beta = 2.2, 2.3, 2.4$. The corresponding string tensions in lattice units [28] are, respectively, equal to $\sigma a^2 = 0.220(9), 0.136(2)$ and $0.071(1)$.

The minimal (lattice) Landau gauge is implemented using the stochastic overrelaxation algorithm [45, 46, 47]. We stop the gauge fixing when the average value of $(\nabla \cdot A)^2$ — see Eq. (6.1) in [47] for a definition — is smaller than 10^{-13} . The gluon and ghost propagators in momentum space are evaluated using the relations

$$D(0) = \frac{1}{12} \sum_{b,\mu} D_{\mu\mu}^{bb}(0) \quad (32)$$

$$D(\tilde{q}) = \frac{1}{9} \sum_{b,\mu} D_{\mu\mu}^{bb}(\tilde{q}) \quad (33)$$

$$G(\tilde{q}) = \frac{1}{3} \sum_b G^{bb}(\tilde{q}), \quad (34)$$

where

$$D_{\mu\nu}^{bc}(\tilde{q}) = \frac{1}{V} \sum_{x,y} \exp[i\tilde{q}(x-y)] \langle A_\mu^b(x) A_\nu^c(y) \rangle, \quad (35)$$

$$G^{bc}(\tilde{q}) = \langle (M^{-1})^{bc}(\tilde{q}) \rangle, \quad (36)$$

$$(M^{-1})^{bc}(\tilde{q}) = \frac{1}{V} \sum_{x,y} \exp[-i\tilde{q}(x-y)] (M^{-1})_{xy}^{bc}, \quad (37)$$

V is the lattice volume and M_{xy}^{bc} is a lattice discretization of the Faddeev-Popov operator $[(-\partial + A) \cdot \partial]$. The expression of this matrix in terms of the gauged-fixed link variables can be found in [48, eq. (B.18)] for the generic $SU(N_c)$ case and in [49, eq. (11)] for the $SU(2)$ case considered in the present work. Let us recall that this matrix has a trivial null eigenvalue corresponding to a constant eigenvector. Thus, one can evaluate the inverse of M_{xy}^{bc} only in the space orthogonal to constant vectors, i.e. at non-zero momentum. For the inversion we used a conjugate gradient method with even/odd preconditioning.

Finally, in order to check for possible Gribov-copy effects we have done (for each thermalized configuration) a second gauge fixing using the smearing method introduced in [50]. To this end we have applied the APE smearing process

$$U_\mu(x) \rightarrow (1 - w) U_\mu(x) + w \Sigma_\mu^\dagger(x), \quad (38)$$

where $\Sigma_\mu(x)$ represents the sum over the connecting staples for the link $U_\mu(x)$, followed by a reunitarization of the link matrix. We have chosen $w = 10/6$ and stopped the smearing when the condition

$$\frac{Tr}{2} \overline{W}_{1,1} \geq 0.995 \quad (39)$$

was satisfied. (This is usually achieved with a few APE-smearing sweeps.) Here $W_{1,1}$ is the 1×1 loop and the average is taken over all $W_{1,1}$ loops of a given configuration. The gauge fixing for the smeared configuration as well as the final gauge-fixing step have been done again using the stochastic overrelaxation algorithm. The smeared gauge-fixing method is supposed to find a unique Gribov copy, even though this copy does not always correspond to the absolute minimum of the minimizing functional [50]. In our simulations we found that the number of *different* Gribov copies obtained with the smeared gauge fixing increases with larger lattice volumes and with smaller β values (see Table II). This is in agreement with previous studies [51, 52, 53] and it should be related to an increasing number of local

	V = 4 ⁴	V = 8 ⁴	V = 16 ⁴
$\beta = 2.2$	4.3 %	25.0 %	97.2 %
$\beta = 2.3$	4.4 %	16.8 %	72.8 %
$\beta = 2.4$	4.1 %	9.8 %	50.8 %

Table II: Percentage of configurations for which the smeared gauge fixing has found a (different) Gribov copy. Results are reported for the three lattice volumes and the three β values considered.

minima for the minimizing function when the system is highly disordered. We also found that the minimum obtained with the smeared gauge fixing is not always smaller than the one obtained without smearing, but at larger lattice volumes the smearing approach seems to be more effective in getting closer to the absolute minimum of the minimizing function (see Table III).

A. Ghost-Gluon Vertex on the Lattice

On the lattice, the definition of the vertex renormalization function is obtained as was done in the continuum (see Section II). The only difference is that, from the weak-coupling expansion (or “perturbative” expansion) on the lattice, one obtains that the ghost-gluon vertex is given at tree level by [54]

$$\Gamma_{\mu}^{abc}(\tilde{k}, \tilde{q}) = i g_0 f^{abc} \hat{q}_{\mu} \cos\left(\frac{\pi \tilde{s}_{\mu} a}{L_{\mu}}\right), \quad (40)$$

	V = 4 ⁴	V = 8 ⁴	V = 16 ⁴
$\beta = 2.2$	46.5 %	52.0 %	63.8 %
$\beta = 2.3$	38.6 %	52.2 %	65.4 %
$\beta = 2.4$	39.0 %	48.7 %	65.4 %

Table III: Percentage of (different) Gribov copies for which the smeared gauge fixing has found a smaller value of the minimizing function. Results are reported for the three lattice volumes and the three β values considered.

where $\tilde{s} = \tilde{k} + \tilde{q}$. Clearly, by taking the formal continuum limit $a \rightarrow 0$ of the quantity $\Gamma_\mu^{abc}(\tilde{k}, \tilde{q})/a$ one recovers the continuum tree-level result (13). Then, in the case $\tilde{k} = 0$, $\tilde{s} = \tilde{q}$, eq. (22) is still valid on the lattice if one sets

$$\Xi(\tilde{q}) = \frac{-i}{\tilde{q}^2} \sum_\mu \frac{\hat{q}_\mu}{\cos\left(\frac{\pi \tilde{q}_\mu a}{L_\mu}\right)} \Gamma_\mu(0, \tilde{q}) \quad (41)$$

with

$$\Gamma_\mu(0, \tilde{q}) = \frac{1}{g_0 N_c (N_c^2 - 1)} \sum_{a,b,c} f^{abc} \Gamma_\mu^{abc}(0, \tilde{q}) \quad (42)$$

$$\Gamma_\mu^{abc}(0, \tilde{q}) = \frac{G_\mu^{abc}(0, \tilde{q})}{D(0) G^2(\tilde{q})} \quad (43)$$

and

$$\hat{q} = \left(\sum_{\mu=1}^4 \hat{q}_\mu^2 \right)^{1/2}, \quad (44)$$

where \hat{q}_μ is defined in terms of \tilde{q}_μ in eq. (31). Thus, as in the continuum, we can write

$$\Xi(\tilde{q}) = \frac{1}{g_0 N_c (N_c^2 - 1)} \frac{1}{\tilde{q}^2} \sum_\mu \frac{\hat{q}_\mu}{\cos\left(\frac{\pi \tilde{q}_\mu a}{L_\mu}\right)} \sum_{a,b,c} f^{abc} \text{Im} \Gamma_\mu^{abc}(0, \tilde{q}). \quad (45)$$

In order to check for possible effects due to the breaking of rotational symmetry, in our simulations we use two types of lattice momenta, i.e. $\tilde{q}_1 = \tilde{q}_2 = \tilde{q}_3 = 0$, $\tilde{q}_4 = \tilde{q}$ and $\tilde{q}_1 = \tilde{q}_2 = \tilde{q}_3 = \tilde{q}_4 = \tilde{q}$. In the following we will indicate the first type of momenta as *asymmetric* and the second one as *symmetric*. Clearly, using the relations $L_1 = L_2 = L_3 = L_4 = L$, we have

$$\hat{q} = \hat{q}_4 = 2 \sin\left(\frac{\pi \tilde{q} a}{L}\right) \quad (46)$$

in the asymmetric case and

$$\hat{q}_\mu = 2 \sin\left(\frac{\pi \tilde{q} a}{L}\right) \quad (47)$$

$$\hat{q} = 4 \sin\left(\frac{\pi \tilde{q} a}{L}\right) \quad (48)$$

in the symmetric one. Then, the quantity $\Xi(\tilde{q})$ above becomes

$$\Xi(\tilde{q}) = \frac{1}{g_0 N_c (N_c^2 - 1)} \frac{1}{\tilde{q}} \frac{1}{\cos\left(\frac{\pi \tilde{q} a}{L}\right)} \sum_{a,b,c} f^{abc} \text{Im} \Gamma_4^{abc}(0, \tilde{q}) \quad (49)$$

in the asymmetric case and

$$\Xi(\tilde{q}) = \frac{1}{g_0 N_c (N_c^2 - 1)} \frac{1}{\tilde{q}} \frac{1}{2 \cos\left(\frac{\pi \tilde{q} a}{L}\right)} \sum_\mu \sum_{a,b,c} f^{abc} \text{Im} \Gamma_\mu^{abc}(0, \tilde{q}) \quad (50)$$

in the symmetric one. Using the trigonometric relation $\sin(2\theta) = 2 \sin(\theta) \cos(\theta)$ these formulae can be rewritten as

$$\Xi(\tilde{q}) = \frac{1}{\sin\left(\frac{2\pi\tilde{q}a}{L}\right)} \Sigma(\tilde{q}) , \quad (51)$$

where

$$\Sigma(\tilde{q}) = \frac{1}{g_0 N_c (N_c^2 - 1)} \sum_{a,b,c} f^{abc} \text{Im} \Gamma_4^{abc}(0, \tilde{q}) \quad (52)$$

in the asymmetric case and

$$\Sigma(\tilde{q}) = \frac{1}{g_0 N_c (N_c^2 - 1)} \sum_{a,b,c} f^{abc} \text{Im} \frac{1}{4} \sum_{\mu} \Gamma_{\mu}^{abc}(0, \tilde{q}) \quad (53)$$

in the symmetric one.

Finally, using eqs. (10), (11) and (37) we obtain

$$G_{\mu}^{abc}(0, \tilde{q}) = V \langle A_{\mu}^a(0) (M^{-1})^{bc}(\tilde{q}) \rangle , \quad (54)$$

where

$$A_{\mu}^a(0) = \frac{1}{V} \sum_x A_{\mu}^a(x) \quad (55)$$

and V is the lattice volume. Then, we can write

$$\Gamma_{\mu}^{abc}(0, \tilde{q}) = \frac{V \langle A_{\mu}^a(0) (M^{-1})^{bc}(\tilde{q}) \rangle}{D(0) G^2(\tilde{q})} . \quad (56)$$

With our notation, in the naive continuum limit $a \rightarrow 0$, the lattice quantity $4 a^2 D(\tilde{q})/g_0^2$ [respectively $a^2 G(\tilde{q})$] approaches the (continuum) propagator $D(q^2)$ [respectively $G(q^2)$]. At the same time, we have that $2 A_{\mu}^a(0)/(a g_0) \rightarrow A_{\mu}^a(0)$ and $a^2 (M^{-1})^{bc}(\tilde{q}) \rightarrow (M^{-1})^{bc}(q)$. This implies that the (normalized) lattice ghost-gluon vertex $g_0 \Gamma_{\mu}^{abc}(0, \tilde{q})/(2 a)$ approaches the quantity $\Gamma_{\mu}^{abc}(0, q)$ in the continuum limit. Also, since $\hat{q} \rightarrow a q$ when $a \rightarrow 0$, it is easy to verify that $\tilde{Z}_1^{-1}(\tilde{q}) = \Xi(\tilde{q})$ is dimensionless.

As said in the Introduction, in Ref. [28] the ghost-gluon renormalization function $\tilde{Z}_1(p^2)$ was indirectly evaluated. To this end the authors considered eq. (1), which can be written as

$$Z_3(p^2, \beta) \tilde{Z}_3^2(p^2, \beta) = \frac{\alpha_s(p^2)}{\alpha_0(\beta)} \tilde{Z}_1^2(p^2, \beta) , \quad (57)$$

where the β dependence is now indicated explicitly. The renormalization functions $Z_3(p^2, \beta)$ and $\tilde{Z}_3^2(p^2, \beta)$ can be evaluated using the matching technique described in detail in [55, Sec.

III]. Then, one can show [28] that the left-hand side of the above equation rises linearly with $-\ln(\sigma a^2)$, where σ is the string tension. At the same time, for large enough β values one finds that [28]

$$\frac{1}{\alpha_0(\beta)} \propto -\ln(\sigma a^2) + \text{constant}, \quad (58)$$

where the constant is β -independent. It follows that $\tilde{Z}_1^2(p^2, \beta)$ must be finite in the continuum limit, if the renormalized coupling $\alpha_s(p^2)$ is assumed finite. Of course, this approach does not allow either an effective determination of the vertex renormalization function or a study of its p dependence. These are the main goals of the present work.

IV. RESULTS

We have evaluated the reduced ghost-gluon vertex function $\Gamma_\mu^{abc}(0, \tilde{p})$ at the asymmetric point $(0; \tilde{p}, -\tilde{p})$ using eq. (56), in the $SU(2)$ case. (Let us recall that when $N_c = 2$ the structure functions f^{abc} are given by the completely anti-symmetric tensor ϵ^{abc} .) Results for the quantity $\Sigma(\tilde{p})$, defined in eqs. (52) and (53), and for $\tilde{Z}_1^{-1}(\tilde{p}) = \Xi(\tilde{p})$ [see eq. (51)] as a function of $p = \hat{p}/a$ (in physical units) are reported in Figs. 4 and 5. We consider for these figures the lattice volume $V = 16^4$, for both asymmetric and symmetric momenta. Error bars were obtained using the bootstrap method with 250 samples. (We checked that the results do not change when considering 500 samples.) We find that the function $\Sigma(\tilde{p})$ has the same momentum dependence as the tree-level vertex [i.e. $\sim \hat{p} \cos(\pi \tilde{p} a/L) \sim \sin(2\pi \tilde{p} a/L)$] and that (consequently) $\tilde{Z}_1(\tilde{p})$ is approximately constant and equal to 1.

As explained in Section III above, in order to check for Gribov-copy effects we have considered two different gauge fixing methods for each thermalized configuration, the second of which employs the so-called smeared gauge fixing. Let us recall that Gribov-copy effects have been found for the ghost propagator in Landau gauge, at least in the small-momentum limit [35, 52, 53, 56]. Recently, such effects were also found for the gluon propagator in the infrared region [57]. In Fig. 5 are also shown the data for $\tilde{Z}_1^{-1}(\tilde{p})$ obtained for the lattice volume $V = 16^4$ using the smeared gauge-fixing. The $\tilde{Z}_1^{-1}(\tilde{p})$ data for all lattice volumes and β values considered in this work are reported in Tables IV (asymmetric momenta) and V (symmetric momenta) considering the two different gauge-fixing methods (without and with smearing). We can clearly see that $\tilde{Z}_1^{-1}(\tilde{p})$ decreases as the lattice volume increases for a fixed coupling β and that for $V = 16^4$ the dependence of $\tilde{Z}_1^{-1}(\tilde{p})$ on the coupling β , on the

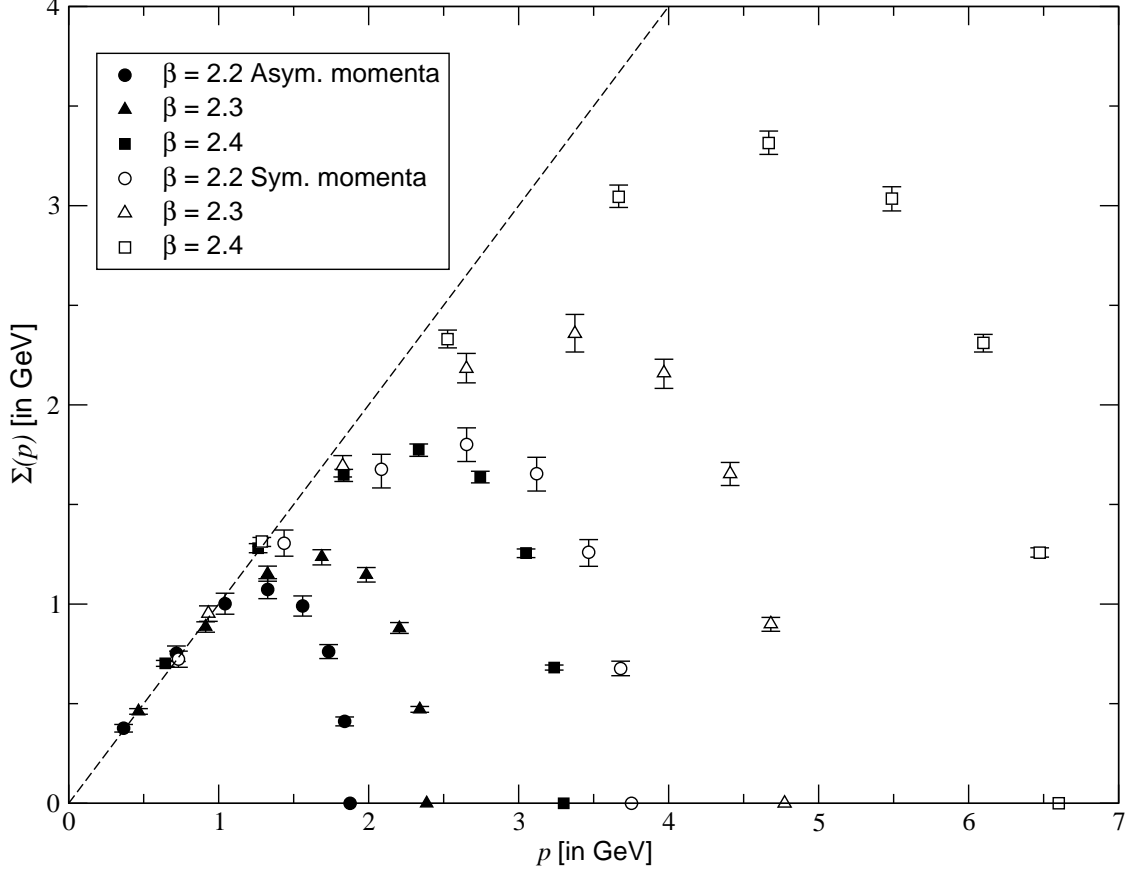


Figure 4: Results for $\Sigma(p)$ for the lattice volume $V = 16^4$ as a function of $p = \hat{p}/a$ in GeV, considering asymmetric and symmetric momenta. Error bars were obtained using the bootstrap method with 250 samples. The dashed line represents the tree-level momentum dependence ($\sim p$) of the vertex function in the continuum.

type of momenta and on Gribov-copy effects is relatively small. This is also evident if we try to fit the data for $\tilde{Z}_1^{-1}(\tilde{p})$ to a constant (see Table VI). Nevertheless, it is clear that data obtained using the smeared gauge-fixing are generally smaller than those obtained without smearing.

It is difficult to explain the small variations in the results for $\tilde{Z}_1^{-1}(\tilde{p})$ when considering asymmetric and symmetric momenta or the smeared gauge fixing compared to the standard gauge fixing. Indeed, several quantities enter the definition of $\Gamma_\mu^{abc}(0, \tilde{p})$ [see eq. (56)] and therefore the evaluation of $\tilde{Z}_1^{-1}(\tilde{p})$. A more detailed study (see Tables VII, VIII and IX) of the gluon propagator at zero momentum $D(0)$, the ghost propagator $G(\tilde{p})$ for $\tilde{p}_1 = \tilde{p}_2 = \tilde{p}_3 = 0, \tilde{p}_4 = N/2$ and the quantity $\sum_{a,b,c} f^{abc} \text{Im} \langle A_\mu^a(0) (M^{-1})^{bc}(\tilde{p}) \rangle$ as a function of $p = \hat{p}/a$

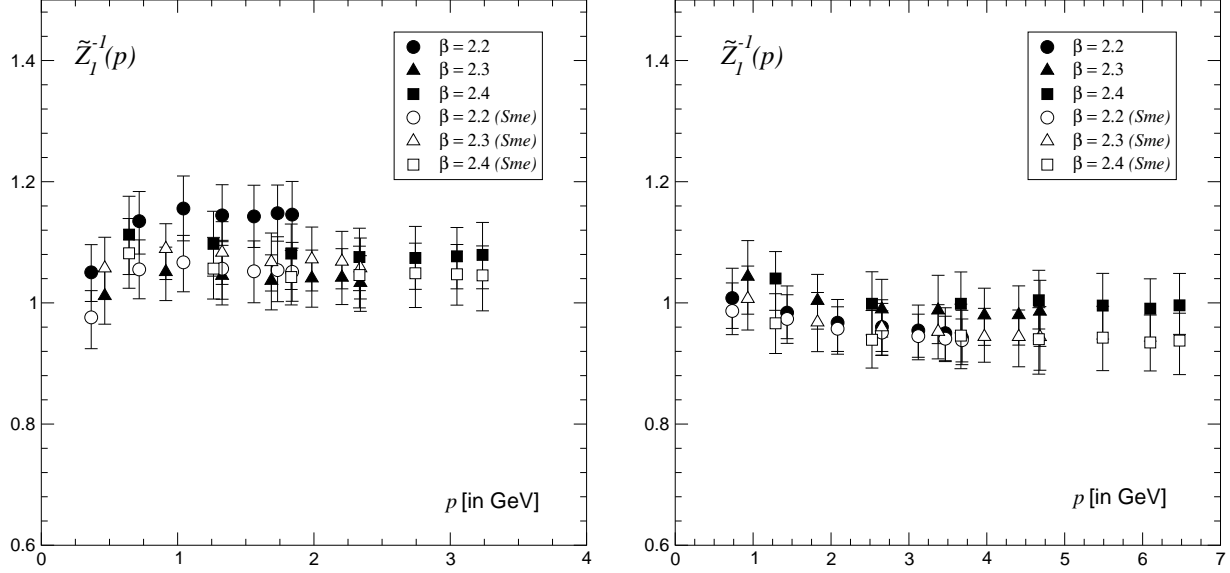


Figure 5: Results for $\tilde{Z}_1^{-1}(p)$ for the lattice volume $V = 16^4$ as a function of $p = \hat{p}/a$ in GeV, considering asymmetric (left) and symmetric (right) momenta. In both cases we show data obtained considering the two different gauge-fixing methods (without and with smearing). Error bars were obtained using the bootstrap method with 250 samples.

does not clarify the situation. In particular, the Gribov-copy effects, if present, are always small and within error bars. This is not surprising, since we are considering relatively small lattice volumes in the scaling region. We can conclude that the small systematic variations in the results of $\tilde{Z}_1(\tilde{p})$ are probably related to correlations among data at different momenta, since they have been obtained using the same set of configurations.

Finally, we can use our data to evaluate the running coupling constant $\alpha_s(p^2)$ using eq. (1). For $\tilde{Z}_1(p^2)$ we take the fit to a constant reported in Table VI. The results are shown in Fig. 6. We can see that data obtained at different β values do not lie on a single curve. This is probably related to the fact that our data are not at infinite volume. Indeed, this is a well-known effect for the gluon field when evaluated at zero momentum [58, 59, 60, 61, 62].

V. CONCLUSIONS

We have studied the reduced ghost-gluon vertex function $\Gamma_\mu^{abc}(0, p)$ and the renormalization function $\tilde{Z}_1(p^2)$ in minimal Landau gauge at the asymmetric point $(0; p, -p)$ in the $SU(2)$ case. We found that the vertex function has the same momentum dependence of

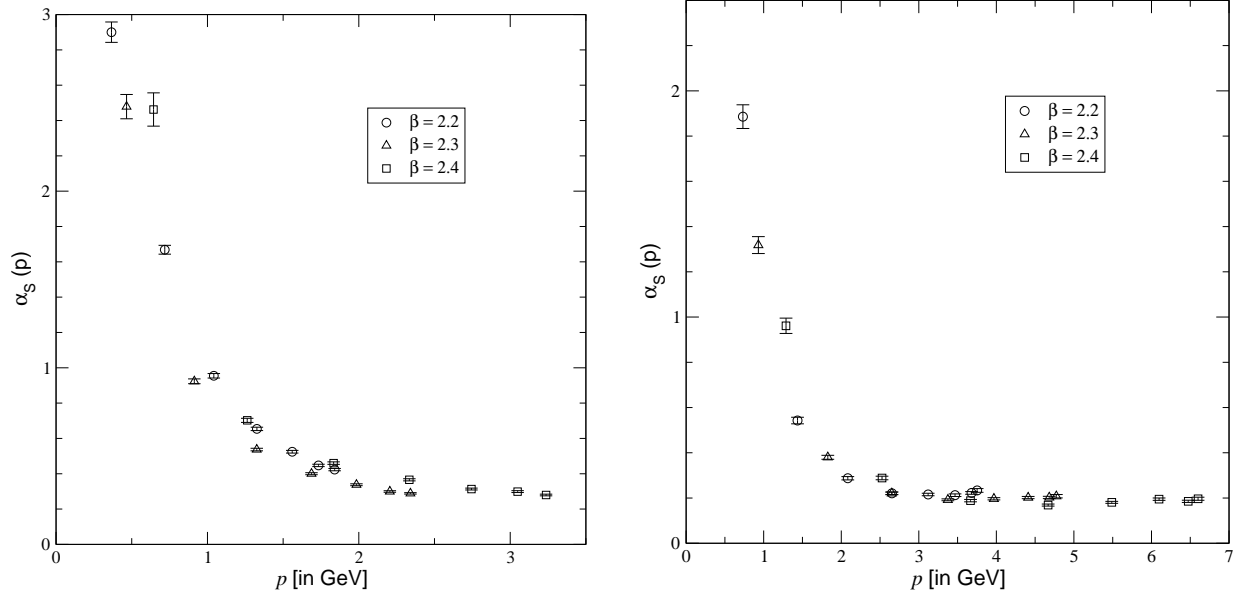


Figure 6: Results for the running coupling $\alpha_s(p)$ as a function $p = \hat{p}/a$ in GeV, considering asymmetric (left) and symmetric (right) momenta. Here we use the standard gauge-fixing method (without smearing). Error bars were obtained using the bootstrap method with 250 samples.

the tree-level vertex and that $\tilde{Z}_1(p^2)$ is approximately constant and equal to 1, at least for momenta $p \gtrsim 1$ GeV. This is a direct non-perturbative verification of the well-known perturbative result that $\tilde{Z}_1(p^2)$ is finite and constant to all orders of perturbation theory [2, 3]. In particular, using the result obtained at the largest value of β considered here (i.e. $\beta = 2.4$) we can write $\tilde{Z}_1^{-1}(p^2) = 1.02^{+6}_{-7}$ (see Table VI), where errors include Gribov-copy effects and discretization errors related to the breaking of rotational invariance.

We are now extending this study, considering larger lattice volumes (and therefore smaller momenta), the symmetric point $k^2 = q^2 = s^2$, the $3d$ case and the $SU(3)$ gauge group. A significant improvement of our results for $\alpha_s(p^2)$ may be expected by considering the symmetric point.

Acknowledgments

This work was supported by Fundação de Amparo à Pesquisa do Estado de São Paulo (FAPESP) through grants: 00/05047-5 (AC, TM) and 03/00928-1 (AM). Partial support from Conselho Nacional de Desenvolvimento Científico e Tecnológico (CNPq) is also ac-

knowledge (AC, TM).

-
- [1] *Foundations of Quantum Chromodynamics*, T. Muta (World Scientific, Singapore, 1987).
 - [2] J. C. Taylor, Nucl. Phys. B **33** (1971) 436.
 - [3] O. Piguet and S. P. Sorella, Lect. Notes Phys. **M28** (1995) 1.
 - [4] L. von Smekal, R. Alkofer and A. Hauck, Phys. Rev. Lett. **79** (1997) 3591.
 - [5] L. von Smekal, A. Hauck and R. Alkofer, Annals Phys. **267** (1998) 1 [Erratum-ibid. **269** (1998) 182].
 - [6] D. Atkinson and J. C. R. Bloch, Phys. Rev. D **58** (1998) 094036.
 - [7] D. Atkinson and J. C. R. Bloch, Mod. Phys. Lett. A **13** (1998) 1055.
 - [8] J. C. R. Bloch, Phys. Rev. D **64** (2001) 116011.
 - [9] D. Zwanziger, Phys. Rev. D **65** (2002) 094039.
 - [10] C. Lerche and L. von Smekal, Phys. Rev. D **65** (2002) 125006.
 - [11] C. S. Fischer and R. Alkofer, Phys. Lett. B **536** (2002) 177.
 - [12] C. S. Fischer, R. Alkofer and H. Reinhardt, Phys. Rev. D **65** (2002) 094008.
 - [13] R. Alkofer, W. Detmold, C. S. Fischer and P. Maris, hep-ph/0309077.
 - [14] R. Alkofer, W. Detmold, C. S. Fischer and P. Maris, hep-ph/0309078.
 - [15] D. Zwanziger, Phys. Rev. D **67** (2003) 105001.
 - [16] J. C. R. Bloch, Few Body Syst. **33** (2003) 111.
 - [17] J. M. Pawłowski, D. F. Litim, S. Nedelko and L. von Smekal, hep-th/0312324.
 - [18] K. I. Kondo, hep-th/0303251.
 - [19] K. I. Kondo, Nucl. Phys. Proc. Suppl. **129** (2004) 715.
 - [20] R. F. Sobreiro, S. P. Sorella, D. Dudal and H. Verschelde, Phys. Lett. B **590** (2004) 265.
 - [21] R. F. Sobreiro, S. P. Sorella, D. Dudal and H. Verschelde, hep-th/0406161.
 - [22] A.C. Aguilar, Ph.D. thesis, IFT–Universidade Estadual Paulista, March 2004 (in Portuguese).
 - [23] A. C. Aguilar and A. A. Natale, hep-ph/0405024.
 - [24] C. S. Fischer and H. Gies, hep-ph/0408089.
 - [25] A. Cucchieri, T. Mendes and D. Zwanziger, Nucl. Phys. Proc. Suppl. **106** (2002) 697.
 - [26] J. C. R. Bloch, A. Cucchieri, K. Langfeld and T. Mendes, Nucl. Phys. Proc. Suppl. **119** (2003) 736.

- [27] K. Langfeld et al., **hep-th/0209173**, in the Proceedings of *Gargnano 2002, Quark confinement and the hadron spectrum*, edited by N. Brambilla and G. M. Prosperi (World Scientific, River Edge, 2003) 297–299.
- [28] J. C. R. Bloch, A. Cucchieri, K. Langfeld and T. Mendes, Nucl. Phys. B **687** (2004) 76.
- [29] D. B. Leinweber, J. I. Skullerud, A. G. Williams and C. Parrinello [UKQCD Collaboration], Phys. Rev. D **60** (1999) 094507 [Erratum-ibid. D **61** (2000) 079901].
- [30] D. R. Bonnet et al., Phys. Rev. D **64** (2001) 034501.
- [31] H. Nakajima and S. Furui, Nucl. Phys. Proc. Suppl. **119** (2003) 730.
- [32] H. Nakajima and S. Furui, **hep-lat/0303024**, in the Proceedings of *Nagoya 2002, Strong coupling gauge theories and effective field theories*, edited by M. Harada et al. (World Scientific, River Edge, 2003) 67–73.
- [33] S. Furui and H. Nakajima, **hep-lat/0309166**.
- [34] S. Furui and H. Nakajima, Phys. Rev. D **69** (2004) 074505.
- [35] H. Nakajima and S. Furui, Nucl. Phys. Proc. Suppl. **129** (2004) 730.
- [36] S. Furui and H. Nakajima, **hep-lat/0403021**.
- [37] S. Furui and H. Nakajima, **hep-lat/0012017**, in the Proceedings of *Wien 2000, Quark confinement and the hadron spectrum*, edited by W. Lucha and K. M. Maung (World Scientific, Singapore, 2001) 275–278.
- [38] A. Mihara, A. Cucchieri and T. Mendes, **hep-lat/0408021**, presented at the *IX Hadron Physics and VII Relativistic Aspects of Nuclear Physics Workshops*, Angra dos Reis, Rio de Janeiro, Brazil (March 28–April 3, 2004).
- [39] R. Alkofer and L. von Smekal, Phys. Rept. **353** (2001) 281.
- [40] A. Cucchieri, T. Mendes, G. Travieso and A. R. Taurines, **hep-lat/0308005**, in the Proceedings of the *15th Symposium on Computer Architecture and High Performance Computing*, São Paulo SP, Brazil, 2003, edited by L.M. Sato et al. (IEEE Computer Society Press, Los Alamitos CA, 2003) 123–131.
- [41] M. Creutz, Phys. Rev. D **21** (1980) 2308.
- [42] S. L. Adler, Nucl. Phys. Proc. Suppl. **9** (1989) 437.
- [43] F. R. Brown and T. J. Woch, Phys. Rev. Lett. **58**, 2394 (1987).
- [44] U. Wolff, Phys. Lett. B **288**, 166 (1992).
- [45] A. Cucchieri and T. Mendes, Nucl. Phys. B **471** (1996) 263.

- [46] A. Cucchieri and T. Mendes, Nucl. Phys. Proc. Suppl. **53** (1997) 811.
- [47] A. Cucchieri and T. Mendes, Comput. Phys. Commun. **154** (2003) 1.
- [48] D. Zwanziger, Nucl. Phys. B **412** (1994) 657.
- [49] A. Cucchieri, Nucl. Phys. B **521** (1998) 365.
- [50] J. E. Hetrick and P. de Forcrand, Nucl. Phys. Proc. Suppl. **63** (1998) 838.
- [51] P. Marenzoni and P. Rossi, Phys. Lett. B **311** (1993) 219.
- [52] A. Cucchieri, Nucl. Phys. B **508** (1997) 353.
- [53] A. Cucchieri and T. Mendes, Nucl. Phys. Proc. Suppl. **63** (1998) 841.
- [54] H. Kawai, R. Nakayama and K. Seo, Nucl. Phys. B **189** (1981) 40.
- [55] A. Cucchieri, T. Mendes and A. R. Taurines, Phys. Rev. D **67** (2003) 091502.
- [56] T. D. Bakeev, E. M. Ilgenfritz, V. K. Mitrjushkin and M. Mueller-Preussker, Phys. Rev. D **69** (2004) 074507.
- [57] P. J. Silva and O. Oliveira, Nucl. Phys. B **690** (2004) 177.
- [58] A. Cucchieri, Phys. Rev. D **60** (1999) 034508.
- [59] A. Cucchieri, Phys. Lett. B **422** (1998) 233.
- [60] A. Cucchieri and D. Zwanziger, Phys. Rev. D **65** (2002) 014001.
- [61] A. Cucchieri and D. Zwanziger, Phys. Lett. B **524** (2002) 123.
- [62] A. Cucchieri, F. Karsch and P. Petreczky, Phys. Rev. D **64** (2001) 036001.

p (GeV)	0.366	0.718	1.04	1.33	1.56	1.73	1.84
$N = 4$	-	-	-	1.40(5)	-	-	-
$N = 4, \text{ sme}$	-	-	-	1.39(4)	-	-	-
$N = 8$	-	1.08(5)	-	1.11(4)	-	1.13(5)	-
$N = 8, \text{ sme}$	-	1.10(5)	-	1.12(4)	-	1.14(4)	-
$N = 16$	1.05(5)	1.13(5)	1.16(5)	1.14(5)	1.14(5)	1.15(5)	1.15(5)
$N = 16, \text{ sme}$	0.98(5)	1.06(5)	1.07(5)	1.06(5)	1.05(5)	1.05(5)	1.05(5)
p (GeV)	0.466	0.913	1.33	1.69	1.98	2.20	2.34
$N = 4$	-	-	-	1.31(4)	-	-	-
$N = 4, \text{ sme}$	-	-	-	1.30(4)	-	-	-
$N = 8$	-	1.30(5)	-	1.22(5)	-	1.21(5)	-
$N = 8, \text{ sme}$	-	1.24(6)	-	1.18(5)	-	1.18(5)	-
$N = 16$	1.01(4)	1.05(4)	1.05(5)	1.04(5)	1.04(5)	1.04(5)	1.03(4)
$N = 16, \text{ sme}$	1.06(5)	1.09(5)	1.08(5)	1.07(5)	1.07(5)	1.07(5)	1.06(5)
p (GeV)	0.644	1.26	1.83	2.34	2.75	3.05	3.24
$N = 4$	-	-	-	1.36(4)	-	-	-
$N = 4, \text{ sme}$	-	-	-	1.35(3)	-	-	-
$N = 8$	-	1.16(5)	-	1.06(5)	-	1.06(4)	-
$N = 8, \text{ sme}$	-	1.15(5)	-	1.07(5)	-	1.06(4)	-
$L = 16$	1.11(6)	1.10(5)	1.08(5)	1.08(5)	1.07(5)	1.08(5)	1.08(5)
$N = 16, \text{ sme}$	1.08(6)	1.06(5)	1.04(5)	1.05(5)	1.05(5)	1.05(5)	1.05(5)

Table IV: Results for $\tilde{Z}_1^{-1}(\tilde{p})$ as a function of $p = \hat{p}/a$ (in GeV) for the three lattice sides $N = 4, 8, 16$ and the three β values considered (i.e. 2.2, 2.3 and 2.4, respectively top, center and bottom part of the table) in the case of asymmetric momenta, considering the two different gauge-fixing methods (without and with smearing). Error bars were obtained using the bootstrap method with 250 samples.

p (GeV)	0.732	1.44	2.08	2.65	3.12	3.47	3.68
$N = 4$	-	-	-	1.22(4)	-	-	-
$N = 4$, sme	-	-	-	1.23(4)	-	-	-
$N = 8$	-	1.07(5)	-	1.01(5)	-	0.99(5)	-
$N = 8$, sme	-	1.03(5)	-	0.98(5)	-	0.97(5)	-
$N = 16$	1.01(5)	0.98(4)	0.97(4)	0.96(4)	0.95(4)	0.95(4)	0.94(5)
$N = 16$, sme	0.99(4)	0.97(4)	0.96(4)	0.95(4)	0.95(4)	0.94(4)	0.94(5)
p (GeV)	0.931	1.83	2.65	3.37	3.97	4.41	4.68
$N = 4$	-	-	-	1.14(4)	-	-	-
$N = 4$, sme	-	-	-	1.12(4)	-	-	-
$N = 8$	-	1.13(6)	-	1.05(5)	-	1.03(5)	-
$N = 8$, sme	-	1.03(5)	-	0.97(5)	-	0.95(5)	-
$N = 16$	1.04(6)	1.00(4)	0.99(5)	0.99(6)	0.98(5)	0.98(5)	0.99(5)
$N = 16$, sme	1.01(5)	0.97(5)	0.96(5)	0.95(4)	0.94(4)	0.94(5)	0.94(5)
p (GeV)	1.29	2.53	3.67	4.67	5.49	6.10	6.48
$N = 4$	-	-	-	1.21(4)	-	-	-
$N = 4$, sme	-	-	-	1.16(4)	-	-	-
$N = 8$	-	1.17(7)	-	1.05(5)	-	1.03(5)	-
$N = 8$, sme	-	1.17(7)	-	1.04(4)	-	1.02(5)	-
$N = 16$	1.04(5)	1.00(5)	1.00(5)	1.00(5)	1.00(5)	0.99(5)	1.00(5)
$N = 16$, sme	0.97(5)	0.94(5)	0.95(5)	0.94(6)	0.94(5)	0.94(5)	0.94(5)

Table V: Results for $\tilde{Z}_1^{-1}(\tilde{p})$ as a function of $p = \hat{p}/a$ (in GeV) for the three lattice sides $N = 4, 8, 16$ and the three β values considered (i.e. 2.2, 2.3 and 2.4, respectively top, center and bottom part of the table) in the case of symmetric momenta, considering the two different gauge-fixing methods (without and with smearing). Error bars were obtained using the bootstrap method with 250 samples.

	asymmetric momenta	symmetric momenta
$\beta = 2.2$	1.148(4)	0.960(6)
$\beta = 2.2$, sme	1.056(4)	0.952(5)
$\beta = 2.3$	1.039(3)	0.989(3)
$\beta = 2.3$, sme	1.070(3)	0.949(5)
$\beta = 2.4$	1.082(4)	1.004(6)
$\beta = 2.4$, sme	1.050(3)	0.946(4)

Table VI: Constant fits of the $\tilde{Z}_1^{-1}(\tilde{p})$ data reported in Tables IV and V for the lattice volume $V = 16^4$ considering momenta $p \geq 1$ GeV.

	$V = 4^4$	$V = 8^4$	$V = 16^4$
$\beta = 2.2$	5.33(6)	11.6(3)	14.5(4)
$\beta = 2.2$, sme	5.38(6)	11.8(2)	14.4(3)
$\beta = 2.3$	6.17(7)	18.9(4)	31.7(7)
$\beta = 2.3$, sme	6.23(7)	19.3(4)	32.4(7)
$\beta = 2.4$	6.87(8)	23.5(5)	53(1)
$\beta = 2.4$, sme	6.94(8)	23.8(5)	53(1)

Table VII: Results for the gluon propagator at zero momentum $D(0)$ (in lattice units) for the three lattice sides ($N = 4, 8, 16$) and the three β values (i.e. 2.2, 2.3 and 2.4) considering the two different gauge-fixing methods (without and with smearing). Error bars were obtained using the bootstrap method with 250 samples.

	$V = 4^4$	$V = 8^4$	$V = 16^4$
$\beta = 2.2$	0.353(1)	0.3174(5)	0.3098(3)
$\beta = 2.2, \text{ sme}$	0.352(1)	0.3175(5)	0.3097(3)
$\beta = 2.3$	0.340(1)	0.3075(4)	0.2998(2)
$\beta = 2.3, \text{ sme}$	0.340(1)	0.3075(4)	0.2997(2)
$\beta = 2.4$	0.334(1)	0.3013(4)	0.2946(3)
$\beta = 2.4, \text{ sme}$	0.333(1)	0.3013(4)	0.2945(3)

Table VIII: Results for the ghost propagator $G(p)$ (in lattice units), evaluated at the asymmetric momentum with components $\tilde{p}_1 = \tilde{p}_2 = \tilde{p}_3 = 0$ and $\tilde{p}_4 = N/2$, for the three lattice sides ($N = 4, 8, 16$) and the three β values (i.e. 2.2, 2.3 and 2.4) considering the two different gauge-fixing methods (without and with smearing). Error bars were obtained using the bootstrap method with 250 samples.

p (GeV)	0.366	0.718	1.04	1.33	1.56	1.73	1.84
$N = 16$	0.28(2)	0.019(1)	0.0041(2)	0.00143(7)	0.00062(3)	0.00029(2)	0.000122(6)
$N = 16, \text{ sme}$	0.26(2)	0.0177(9)	0.0038(2)	0.00131(7)	0.00057(3)	0.00027(1)	0.000111(6)
p (GeV)	0.466	0.913	1.33	1.69	1.98	2.20	2.34
$N = 16$	0.46(3)	0.031(2)	0.0069(4)	0.0025(1)	0.00113(6)	0.00054(3)	0.00023(1)
$N = 16, \text{ sme}$	0.48(4)	0.032(2)	0.0073(4)	0.0026(1)	0.00118(7)	0.00057(3)	0.00024(1)
p (GeV)	0.644	1.26	1.83	2.34	2.75	3.05	3.24
$N = 16$	0.74(7)	0.046(3)	0.0108(6)	0.0040(2)	0.0018(1)	0.00089(5)	0.00037(2)
$N = 16, \text{ sme}$	0.70(6)	0.045(3)	0.0106(6)	0.0039(2)	0.0018(1)	0.00087(5)	0.00037(2)

Table IX: Results for the quantity $\sum_{a,b,c} f^{abc} \text{Im} \langle A_\mu^a(0) (M^{-1})^{bc}(\tilde{p}) \rangle$ as a function of $p = \hat{p}/a$ (in GeV) for the lattice side $N = 16$ and the three β values considered (i.e. 2.2, 2.3 and 2.4, respectively top, center and bottom part of the table) in the case of asymmetric momenta, considering the two different gauge-fixing methods (without and with smearing). Error bars were obtained using the bootstrap method with 250 samples.